AIMS Materials Science, 4(1): 231-249.
DOI: 10.3934/matersci.2017.1.231
Received: 28 November 2016
Accepted: 20 January 2017
Published: 06 February 2017

http://www.aimspress.com/journal/Materials

Research article

Magnetic retardance and magnetic heating in dextran-citrate coated ferrofluids

Jing-Fung Lin [1,*], Jer-Jia Sheu [2], and Xin-Rong Qiu [3]

[1] Department of Industrial Design, Far East University, Taiwan, R.O.C.
[2] Department of Mechanical Engineering, Southern Taiwan University of Science and Technology, Taiwan, R.O.C.
[3] Graduate School of Mechanical Engineering, Far East University, Taiwan, R.O.C.

* **Correspondence:** Email: jacklin@cc.feu.edu.tw; Tel: +886-6-5979566-5364.

Abstract: The Fe_3O_4 magnetic nanoparticles (MNPs) coated by citrate and dextran prepared by the co-precipitation method was described. Influence induced by the mass variation of coating dextran was investigated. Magneto-optical birefringence of biocompatible dextran-citrate (DC) coated ferrofluids (FFs) was obtained by the Stokes polarimeter. Next, uniform design method was used to find the DC coated FF with high retardance and low dichroism. Retardance of the optimized A9 sample with 1 g/ml was measured as 56.7898° (dichroism was 0.3716) under 64.5 mT. Further, magnetic heating effect in alternating magnetic field was investigated. When the concentrations of A9 were of 2 mg/ml and 50 mg/ml, under the external alternating magnetic field with applied apparent current of 210 A, after heating 5 s the temperature of the DC coated FFs was greater than 47 °C, respectively, reached the requirements for the magnetic inductive heating treatment of cancer tumor. The potential of DC coated FFs in hyperthermia was highly evaluated.

Keywords: birefringence; dichroism; ferrofluids; hyperthermia; retardance

1. Introduction

A large variety of biocompatible magnetic nanoparticles (MNPs) have established useful applications in biomedical fields, such as hyperthermia, magnetic resonance imaging (MRI), and drug delivery inside the body [1]. Among the various methods for producing MNPs, the chemical co-precipitation method is frequently used because of its advantages as low cost, simple equipment,

usual raw materials, easy control of the size of the nanoparticles (NPs), and precise control of property and chemical composition of the product.

Due to the high ratio of surface to volume and magnetization, Fe_3O_4 MNPs are prone to aggregate in water or tissue fluid which limits the application [2]. To avoid agglomeration of MNPs due to attractive van der Waals forces, the particles need to be coated with different complex agents that provide enhanced stability due to steric hindrance or combined electrostatic and steric stabilization. Small molecules such as citrate (citric acid, CA), is one of the mostly used coating agents [3–8]. Also, the CA coated ferrofluids (FFs) have been used as feasible thermoseeds in hyperthermia application [3,4] and as a contrast agent in MRI application [5,6]. Effects of synthesis conditions on the properties of CA coated iron oxide NPs were investigated [7,8].

For biocompatible FFs, it was known that the static magnetic birefringence signal includes agglomerates and the particle size polydispersity, the magnetic susceptibility and the relative frequencies of monomer and higher magnetic structures were obtained [4,9]. Via the use of experimental orthogonal design method and the magneto-optical measurements executed by a Stokes polarimeter, the CA coated FF with high saturation magnetism, high retardance, and low dichroism was obtained [8]. Further, in hyperthermia, one seeks to achieve the highest magnetic response due to an applied modulation field, which in turn depends upon the magnetic susceptibility and magnetic moment of the existing magnetic structure [4,9]. Hence it is noteworthy to investigate the magnetic retardance (birefringence) prior to test the heating performance of FF [3,4].

In addition, in order to increase the water dispersibility and the biologic stability in MNPs, MNP coating with polymers such as PEG (polyethylene glycol) [10], dextran [11], albumin, gelatin, chitosan, PVA (polyvinyl alcohol), PLGA (poly lactic-co-glycolic acid) were studied [12]. Among these polymers, dextran, chitosan, and gelatin belong to the natural polymers. Dextran as natural polysaccharide, which is widely used in the pharmaceutical field, has attracted much attention. Dextran is water soluble, inert in biological systems and does not influence cell viability [13]. The preparation of oleyl stabilized MNPs which further chemically modified with CA and subsequently with different polymers including PEG were reported [10]. In the investigation [12], the CA chemically capped MNPs with desirable size, morphology and magnetic properties were synthesized and characterized before the conjugation of PEG. The synthesis of dextran coated MNPs were discussed [14,15,16], and the heating effect (single-domain magnetite particles under high frequency) of dextran-sodium oleate stabilized FFs was studied [16].

Hyperthermia is an important application, which can increase the temperature of tumors to 41~46 °C and therefore kill tumor cells. This method involves the introduction of ferromagnetic or superparamagnetic particles into the tumor tissue and then irradiation with an AC (magnetic field that varies sinusoidally) magnetic field. The transformation efficiency of the energy strongly depends on the frequency and amplitude of the external field as well as the nature of the particles such as magnetism, surface modification, and concentration of FFs [17].

Owing to the stabilized biocompatible CA coated FF was successfully produced with have high retardance and magnetization in our previous study [8]. Also, heating effect induced by the concentration of FFs and the magnetic field intensity on the CA coated FF with the second high retardance was discussed [4]. Moreover, in most of the work carried out in hyperthermia and MRI fields, magnetite or maghemite particles were used, and these particle surfaces were functionalized by biocompatible molecules of citrate [1,3–8,12] and dextran separately [2,11,13–16]. Therefore, the aim of the present paper is to develop the dextran-citrate (DC) coated FFs, and to investigate not only

magnetic retardance but also heating performance of the DC coated FFs in hyperthermia application.

2. Materials and Method

2.1. Materials

Ferric chloride ($FeCl_3$), ferrous sulfate ($FeSO_4 \cdot 7H_2O$), aqueous ammonia (NH_4OH), and ethyl alcohol were all analytic grade. Citric acid ($C_6H_8O_7$, Showa, 99.5%) and deionized water were industrial grade. Dextran (from Leuconostoc spp, Fluka, MR~40000) and dialysis film (molecular weight cut off, MWCO of 40000) were used in this study.

2.2. Synthesis of Dextran-Citrate Coated MNPs

To synthesize Fe_3O_4 MNPs, in a typical experiment, a solution with 25 ml $FeCl_3$ (1.75 mol/L) and 25 ml $FeSO_4 \cdot 7H_2O$ (1 mol/L), respectively, mixed with a molar ratio of 1.75:1 (around ideal ratio of 2:1) was prepared in a three-necked flask without N_2 protection, and was ultrasonically vibrated for 30 min. In a room temperature of 20 °C, 20 ml ammonia aqueous solution (mass ratio of 25%) was then charged into the mixed solution at a rate of 0.15 ml/sec with vigorously mechanical stirring of 1000 rpm and ultrasonic vibration, until the pH value of the solution reached 9. Thereafter, the temperature was raised to 70 °C and the solution was kept on stirring for additional 30 min. The resulted black mixture was collected and washed three times with deionized water and ethyl alcohol, respectively, and until the pH value of mixture was around 7. After magnetic separation, washing, and decanting, the colloidal suspensions of Fe_3O_4 MNPs were obtained.

Further, in a typical experiment for coating CA onto the Fe_3O_4 MNPs, 100 ml deionized water was added to the suspension of 6 g Fe_3O_4 MNPs, and mechanical stirring of 900 rpm and ultrasonic vibration were done for 30 min. Then, mechanical stirring of 900 rpm was still on, and the hydrochloric acid was used to adjust the pH value of the solution to be 5 before coating. While mechanical stirring of 400 rpm was still on and the temperature was raised to 80 °C, the CA solution of 15 g/L (0.3 g CA dissolved in 20 ml deionized water) was dropped into the solution at a rate of 2 ml/min. After the titration of CA solution was over, the reaction was done for a further 30 min. Then the resulted black mixture was collected and washed with deionized water until the pH value was around 7 (the pH value of suspension after surface coating). Finally the ultrasonic vibration was done on the CA coated MNPs contained in deionized water for 15 min, and the stabilized CA coated Fe_3O_4 FFs were obtained [8].

Moreover, in a typical experiment for coating dextran onto the CA coated Fe_3O_4 MNPs, 100 ml deionized water was added to the suspension of 4 g CA coated MNPs, and mechanical stirring of 900 rpm and ultrasonic vibration were done for 30 min. Then, mechanical stirring of 900 rpm was still on, and the hydrochloric acid was used to adjust the pH value of the solution to be 5 before coating. While mechanical stirring of 400 rpm was still on and the temperature was raised to 80 °C, the dextran solution of 30 g/L (0.6 g dextran dissolved in 20 ml deionized water) was dropped into the solution at a rate of 2 ml/min. After the titration of dextran solution was over, the reaction was done for a further 30 min. Then the resulted black mixture was collected and washed with deionized water until the pH value was around 7. Finally the ultrasonic vibration was done on the DC coated MNPs contained in deionized water for 10 min. After the ultrasonic vibration, double centrifugations of

3000 rpm followed by 6000 rpm, respectively, for 20 min and 15 min were adopted. Then the dialysis liquid of 100 ml was used for 1 day and the stabilized DC coated Fe_3O_4 FFs were obtained.

3. Results and Discussion

3.1. Measurement of Retardance and Dichroism in the DC Coated FFs

Considering the effects induced by the mass variation of surfactant as dextran, we adopted 4 g CA coated Fe_3O_4 MNPs and varied the amount of dextran from 0.5 g to 0.7 g in increments of 0.05 g. After producing these DC coated FFs, we used the previously developed Stokes polarimeter for measuring the magneto-optical properties including magnetic-induced retardance and dichroism in FFs [18]. The accuracy of retardance and dichroism measurements was influenced by the reliability and accuracy of Stokes vector measured by a Stokes polarimeter and the function of derived algorithm [18]. The DC coated FF samples (the mass amount of dextran as 0.5 g, 0.55 g, 0.6 g, 0.65 g, and 0.7 g) of 1 g/mL were injected in to a liquid cell with a thickness of 12.5 μm and were then introduced into the measurement system. Figures 1 and 2 presented the results obtained for the retardance and dichroism of the DC coated FF samples under external magnetic field (0 to 1 A in increments of 0.1 A, i.e., from 0 T to 64.5 mT). The propagation direction of the light was normal to the applied transverse magnetic field. Magnetic field was generated by a magnetic generator (U-shaped core, GMBH, Germany).

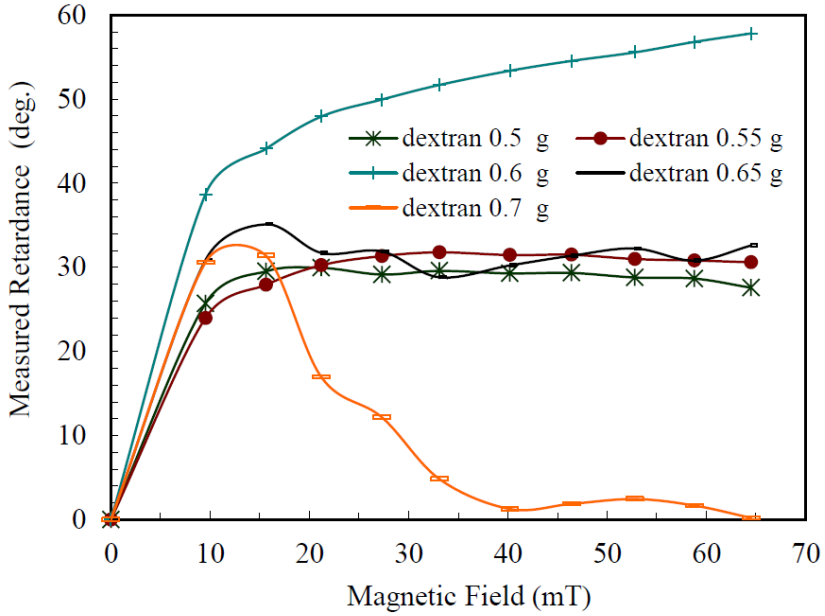

Figure 1. Experimental results of retardance in the DC coated FF samples.

From inspection, as shown in Figure 1, the experimental result showed the magnitude of retardance increased with the increasing magnetic fields for the DC coated FF with 0.6 g dextran. Retardance was measured as 57.82° under magnetic field of 64.5 mT (with calibration of empty cell), which was higher than that of 37.81° for a water-based EMG 304 with a volume concentration of 4.1% [19]. In addition, the retardance of the DC coated FFs with 0.65 g dextran and 0.7 g dextran,

respectively, varied more abruptly than those of the DC coated FFs with 0.5 g dextran and 0.55 g dextran. It might happen from the excess dextran and the agglomerations could occur. And the DC coated FFs with 0.65 g dextran and 0.7 g dextran might have low dispersibility and of high saturation magnetization (70.46 emu/g and 71.72 emu/g, respectively). Hence there are peaks (maximum) retardances corresponding to the DC coated FFs with 0.65 g dextran and 0.7 g dextran, which were observed in the Figure 1. Further, the dispersibilty (colloidal stability) could be certificated by the variation in the absorbance obtained by the UV spectrum or the DLS test. The formation of magnetic-chain arrangement for these DC coated FFs could be observed under high-power microscope. The magnetic-field-induced retardance (magneto-optical response) for the DC coated FFs was significantly influenced by high particle dispersibility and high enough saturation magnetization.

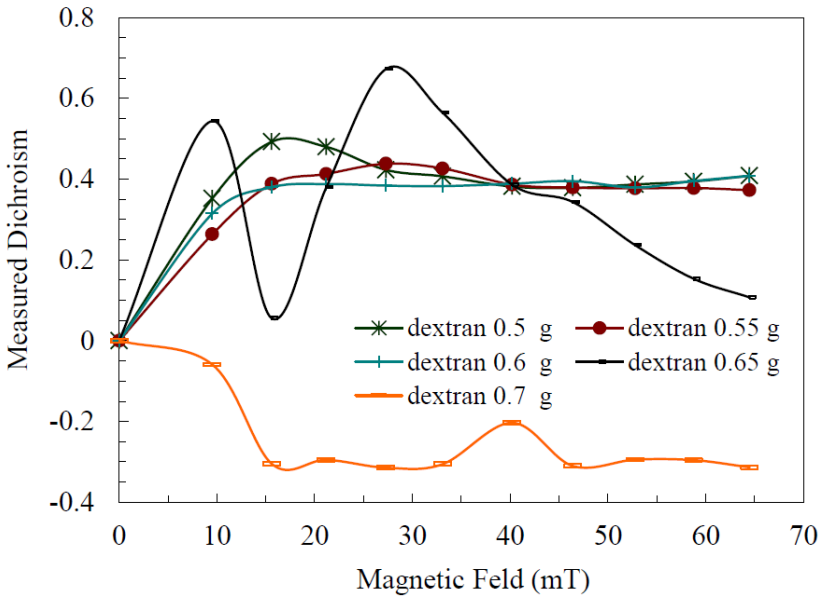

Figure 2. Experimental results of dichroism in the DC coated FF samples.

From inspection, as shown in Figure 2, the magnitude of dichroism increased with the increasing magnetic fields in the initial value and kept non-varied for the DC coated FF sample with 0.6 g dextran. And it was shown that the DC coated FF sample with 0.6 g dextran resulted in absorption (with a value of 0.408 under 64.5 mT) and was much smaller than that of 0.705 for EMG 304 [19]. It was noted that we could not exactly know what the surfactant is in a commercial EMG 304. Further, it was known that the small size, high dispersion, and high saturated magnetization (magnetic response) may dominate the magnetic-field induced birefringence behavior of FFs [18]. Hence, the water-based DC coated FF with high retardance may be suitable to be used in hyperthermia, i.e., the magnetic inductive heating of FFs [4].

Moreover, it was noted that the measured dichroism for these DC coated FFs were calculated by an equation, which was a function of principal axis angle and retardance [18]. The measured principal axis angle for the DC coated FF with 0.6 g dextran was of 21.46° with a standard deviation of 0.11° (it is suggested that the distribution of principal axis angle in 11 measurement times was most uniform among these five FFs samples). The measured principal axis angle for the DC coated

FFs with 0.65 g dextran and 0.7 g dextran was of 23.17° and 23.47° with a standard deviation of 0.57° and 0.63° (large abrupt variation), respectively. Therefore the high peak dichroism in the DC coated FF with 0.65 g dextran might arise. It was noted that results of the measured principal axis angle for these DC coated FFs were not shown in the paper. Indeed, variations of the measured principal axis angle and retardance could have a significant influence on the measured dichroism. And the measured dichroism value and the corresponding variation with magnetic field could be different according to the applied algorithms of various precisions.

Figure 3 showed the Fourier transform infrared (FTIR) spectra of the CA coated Fe_3O_4 and the DC coated Fe_3O_4 with 0.6 g dextran. In Figure 3A, the characteristic peak corresponding to the stretching vibration of Fe–O bond was also shifted to lower wavenumbers of 565.05 cm^{-1} compared to that of 576 cm^{-1} of nano Fe_3O_4 [2,13]. We could say that the citric acid bound to the magnetite surface by carboxylate [2]. Also, the absorption peak at about 3168.5 cm^{-1} could be ascribed to hydroxyls; this showed the surface of iron oxide particles had large numbers of hydroxyls [2,13]. Further, The peaks at 1618.01 cm^{-1} and 1400.1 cm^{-1} corresponding to the asymmetric and symmetric stretching of carboxyl group confirmed the presence of citrate in the CA coated FF [6].

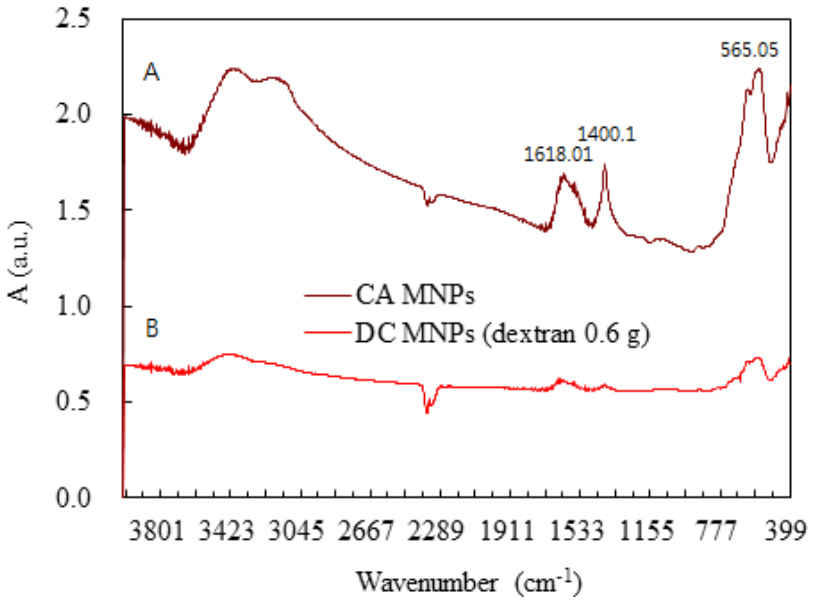

Figure 3. FTIR spectra of the CA coated Fe_3O_4 and the DC coated Fe_3O_4 with 0.6 g dextran.

It is known that the widely used functional groups in polysaccharides available for chemical modification include hydroxyl, amino, aldehyde, and carboxylic acid groups. The hydroxyl group is useful to react with compounds bearing anhydrides, carboxylic acids, or epoxides. Chemical modification is usually performed with the primary hydroxyl group at C6 of the sugar (e.g., dextran, chitosan, and hyaluronic acid) due to the higher reactivity of this position relative to secondary or tertiary moieties. The carboxylic acid and amino groups are frequently reacted by forming the amide bond via carbodiimide-mediated reactions [6,20].

Following the procedure described in section 2.2 for double coating dextran on the anionic CA coated MNPs [12]; the carboxylic functional group of citric acid is converted to covalent bond of ester. Polymer or molecules (such as citrate) containing carboxylic acid groups can be used to

generate a negative charge [21]. It was said that the CA coated suspension with pH = 5 has high dispersibility (pH-dependent colloidal stability) maybe resulted from the high Zeta potentials (surface property) existing on the surface of CA coated MNPs, providing large electrostatic repulsions and steric repulsions between MNPs [8].

Further, generation of positive charges on polymer coated iron oxide NPs generally comes from polymers or molecules containing amine groups (primary, secondary or tertiary) [21]. It is said that the molecules employed for assembly should have a sufficient number of charged groups to provide stable adsorption on an oppositely charged surface and non-compensated charges exposed to the exterior [22]. So there is an optimum molar ratio (weight ratio) between CA and dextran to let the double-layer coated FFs give a good stability through electrostatic or steric repulsion. Also, it is known that the vibration bands for the dextran was found to be rather broad, as expected due to strong intra- and intermolecular hydrogen bonding [1]. For dextran, the vibration bands for the C–O bond ranging from 1040 cm^{-1} to 1150 cm^{-1} and C–H bond ranging from 1250 cm^{-1} to 1460 cm^{-1} [23]. It was found that the peaks at 1043.3 cm^{-1} and 1400.1 cm^{-1} weakened in the curve of Figure 3B. The carboxylic functional group of CA was converted to ester linkage characterized by shifting stretching band from 1618.01 cm^{-1} to a higher frequency (1637.3 cm^{-1}) in FTIR spectrum [12]. Hence, results of Figure 3B (there existed corresponding lower peaks) showed that dextran was successfully coated on the surface of CA MNPs through van der Walls force, hydrogen bond and electrostatic interactions [2].

Moreover, dynamic light scattering (DLS) tests of the CA coated Fe_3O_4 MNPs and the DC coated Fe_3O_4 MNPs synthesized under 0.6 g dextran were shown in Figure 4. In Figure 4(a), it was found that in the case of the CA coated Fe_3O_4, the number distribution was 76.9% (range from 60 nm to 100 nm) and the polydispersity index (PDI) for the hydrodynamic diameters of the CA coated MNPs was determined as 0.216, while in the case of the DC coated Fe_3O_4 MNPs synthesized under 0.6 g dextran as shown in Figure 4(b), the number distribution was 84.5% (range from 60 nm to 100 nm) and the PDI for the hydrodynamic diameters of the DC coated MNPs was determined as low as 0.153.

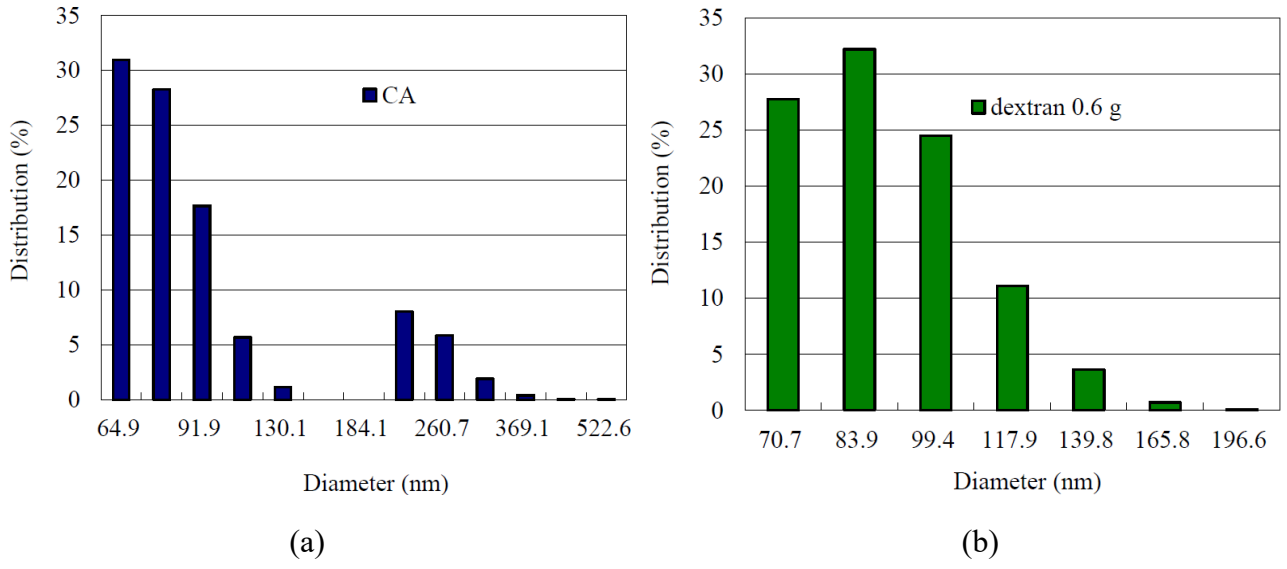

Figure 4. DLS tests (a) of the CA coated Fe_3O_4 and of (b) the DC coated Fe_3O_4 MNPs synthesized under 0.6 g dextran.

Further, via SQUID (superconducting quantum interference device, Quantum Design, MPMS-XL7, USA) measurements at room temperature and magnetic field intensity between −20000 Oe and +20000 Oe, saturation magnetizations of the Fe_3O_4 powder and the CA coated Fe_3O_4 powder were 53.2 emu/g and 49.19 emu/g, respectively, as shown in Figure 5. Also, the saturation magnetizations of the DC coated Fe_3O_4 powders with dextran amounts of 0.55 g, 0.6 g, and 0.65 g were obtained as 40.06 emu/g, 60.07 emu/g, and 70.46 emu/g, respectively.

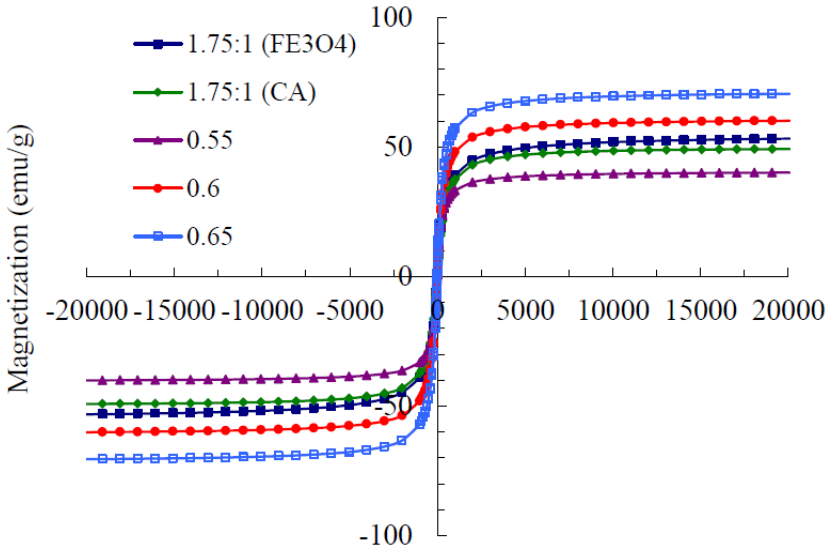

Figure 5. Magnetization curves of the DC/CA coated Fe_3O_4 MNPs and the pure Fe_3O_4 MNPs.

Saturation magnetization of the DC coated Fe_3O_4 MNPs with 0.6 g dextran is 60.07 emu/g, which was much higher than those of 49.19 emu/g of the CA coated Fe_3O_4 powder and 53.2 emu/g of the pure Fe_3O_4 MNPs. The lower value of magnetization after CA coating was due to the coating of the non-magnetic surfactant layer. In addition, saturation magnetization of the DC coated Fe_3O_4 MNPs with 0.6 g dextran was higher than those of 58.6 emu/g, 54.8 emu/g, 48.1 emu/g, and 38.7 emu/g of dextran coated MMPs at different weight ratio of dextran to magnetite [1]. In addition, low coercivity (Hc) as 2.97 Oe and remanent magnetization (Mr) as 1.002 emu/g were obtained in the DC coated Fe_3O_4 MNPs with 0.6 g dextran. Hence the DC coated Fe_3O_4 MNPs with 0.6 g dextran was highly superparamagnetic.

3.2. Optimization of DC Coated FFs for High Retardance and Low Dichroism Using Uniform Design

Uniform design method (UD) is based on uniform distribution in number theory. It makes experiment points uniformly scattered in the range of experiment parameters for getting more information by less experiment [24]. Similar to Taguchi orthogonal design method (OD), UD defines experiment points by some specially designed UD tables, the details of which can refer to [25,26]. It is known that OD is often used to design and organize the foregoing experiments effectively. Taguchi method is straightforward and easy to apply to many engineering situations, making it a powerful yet simple tool. The optimal synthesis condition of CA coated Fe_3O_4 FF with high retardance was

determined by the OD-$L_9(3^4)$ successfully [8].

Instead, the optimal synthesis condition of the DC coated Fe_3O_4 FF with high retardance and low dichroism was determined by the uniform design method. To explore optimal experimental conditions in multi-factors and multi-levels experiment using uniform experimental design, the factor–level table of uniform design-$U_9(9^4)$ was shown in Table 1 [27,28].

Table 1. The factor–level table of uniform design-$U_9(9^4)$.

Parameter	Level								
	1	2	3	4	5	6	7	8	9
Fe_3O_4 (g/ml)	6/80	6/80	6/90	6/90	6/100	6/100	6/110	6/110	6/120
Temp. (℃)	45	50	55	60	65	70	75	80	85
CA (g)	0.24	0.24	0.24	0.3	0.3	0.3	0.36	0.36	0.36
Dextran (g)	0.55	0.55	0.55	0.6	0.6	0.6	0.65	0.65	0.65

From the investigation of retardance results in the DC coated FFs, as shown in Figure 6, hence the experimental conditions for the A9 sample with high retardance of 56.7898° under 64.5 mT were determined as follows: concentration of Fe_3O_4 was 6 g/120 ml, coating temperature was 85 ℃, 0.36 g CA (dissolved in 20 ml) and 0.65 g dextran (dissolved in 20 ml). Moreover, from the investigation of dichroism results, as shown in Figure 7, the dichroism value for the A9 sample was 0.3716 with the least standard value of 0.0319 among the nine samples. Results of retardance under 64.5 mT and average dichroism value were shown in Table 2 and Table 3, respectively.

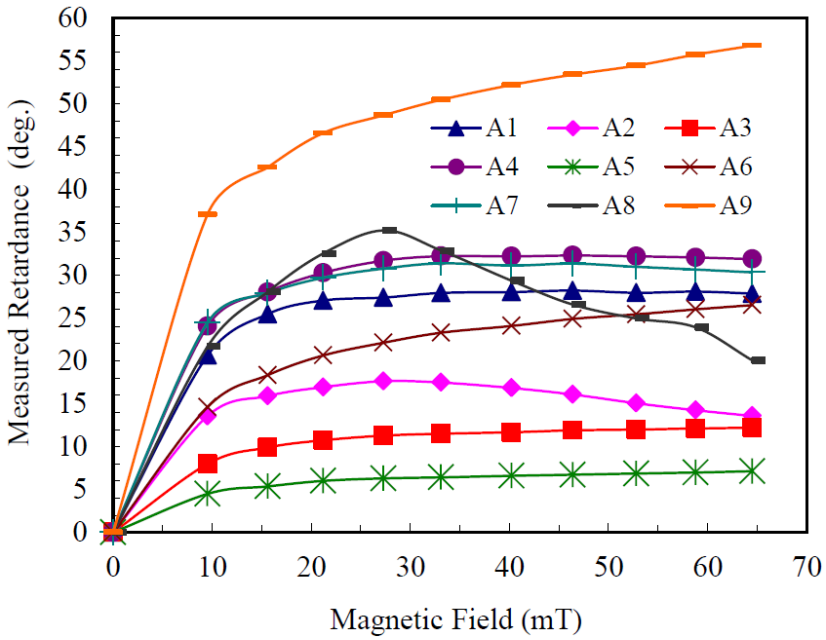

Figure 6. Experimental results of retardance in DC coated FF samples using uniform design method.

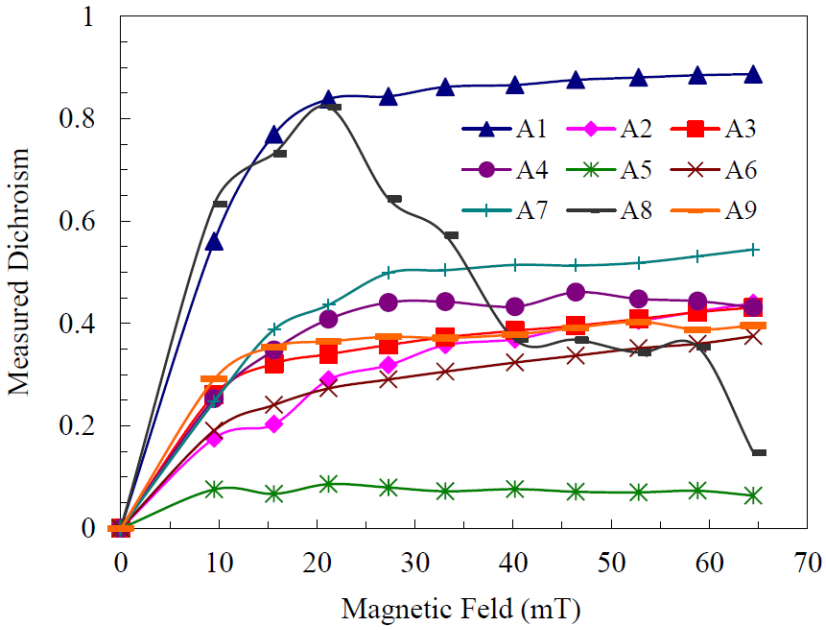

Figure 7. Experimental results of dichroism in DC coated FF samples using uniform design method.

Table 2. Uniform design and test results of retardance.

Test No.	Level of parameter				
	Fe_3O_4 (g/ml)	Temp. (°C)	CA (g)	Dextran (g)	Retardance (deg)
1	1(6/80)	2(50)	4(0.30)	7(0.65)	27.8628
2	2(6/80)	4(60)	8(0.36)	5(0.60)	13.5872
3	3(6/90)	6(70)	3(0.24)	3(0.55)	12.2155
4	4(6/90)	8(80)	7(0.36)	1(0.55)	31.8867
5	5(6/100)	1(45)	2(0.24)	8(0.65)	7.1405
6	6(6/100)	3(55)	6(0.30)	6(0.60)	26.5201
7	7(6/110)	5(65)	1(0.24)	4(0.60)	30.3393
8	8(6/110)	7(75)	5(0.30)	2(0.55)	20.0765
9	9(6/120)	9(85)	9(0.36)	9(0.65)	56.7898

According to the TEM result of the A9 sample (the DC coated Fe_3O_4 MNPs synthesized under the CA coated Fe_3O_4 MNPs), as shown in Figure 8 in 50 nm scales, the sizes of the nearly spherical DC coated Fe_3O_4 MNPs were close to 15 nm. Figure 9 showed the XRD patterns of the A9 sample, it was found that all the different peaks at 2θ = 30.1°, 35.4°, 43.1°, 53.4°, 56.9°, and 62.6° could be well indexed to the inverse cubic spinel structure of Fe_3O_4 [29]. The characteristic peaks of Fe_3O_4 did not disappear. The average crystallite sizes of the A9 sample and CA coated Fe_3O_4 MNPs (for the second peak) were about 12.50 nm and 18.75 nm, respectively. The characteristic peaks of Fe_3O_4 did not disappear for these two samples, demonstrating that the crystal structure of MNPs does not change after surface modification of citric acid [8] and dextran [13,30]. The average crystallite size of the A9 sample for the second peak was about 12.50 nm, which agreed with the magnetic core

particle size viewed under the TEM.

Table 3. Uniform design and test results of dichroism.

Test No.	Level of parameter				
	Fe_3O_4 (g/ml)	Temp. (°C)	CA (g)	Dextran (g)	Dichroism (average)
1	1(6/80)	2(50)	4(0.30)	7(0.65)	0.8267
2	2(6/80)	4(60)	8(0.36)	5(0.60)	0.3378
3	3(6/90)	6(70)	3(0.24)	3(0.55)	0.3698
4	4(6/90)	8(80)	7(0.36)	1(0.55)	0.4111
5	5(6/100)	1(45)	2(0.24)	8(0.65)	0.0738
6	6(6/100)	3(55)	6(0.30)	6(0.60)	0.3050
7	7(6/110)	5(65)	1(0.24)	4(0.60)	0.4697
8	8(6/110)	7(75)	5(0.30)	2(0.55)	0.4986
9	9(6/120)	9(85)	9(0.36)	9(0.65)	0.3716

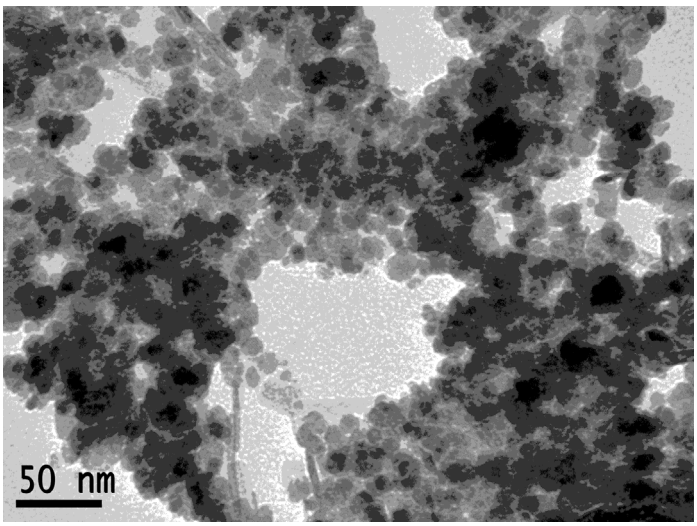

Figure 8. TEM morphology of the A9 sample (the DC coated Fe_3O_4 MNPs synthesized under the CA coated Fe_3O_4 MNPs).

Further, via SQUID measurements at room temperature and magnetic field intensity between −20000 Oe and +20000 Oe, saturation magnetizations of the DC coated Fe_3O_4 powder for the A9 sample and the corresponding CA coated Fe_3O_4 powder were 57.42 emu/g and 64.72 emu/g, respectively, as shown in Figure 10(a). The ratio of saturation magnetization of the CA coated sample to that of the bulk magnetite (92 emu/g) was 70.4%. Low coercivity (Hc) as 11.63 Oe and remanent magnetization (Mr) as 0.95 emu/g were obtained in the CA coated sample.

Moreover, if we zoom in the magnetization curve that is close to the zero, as shown in Figure 10(b), low coercivity (Hc) as 10.90 Oe and remanent magnetization (Mr) as 1.278 emu/g were obtained in the A9 sample. Therefore the A9 sample could be said to have excellent

superparamagnetization for the remanent magnetization close to zero and low coercivity. Accordingly, high linear birefringence and low dichroism of the A9 sample were evidenced by the narrow particle distribution, high dispersibility, and high saturation magnetization [31].

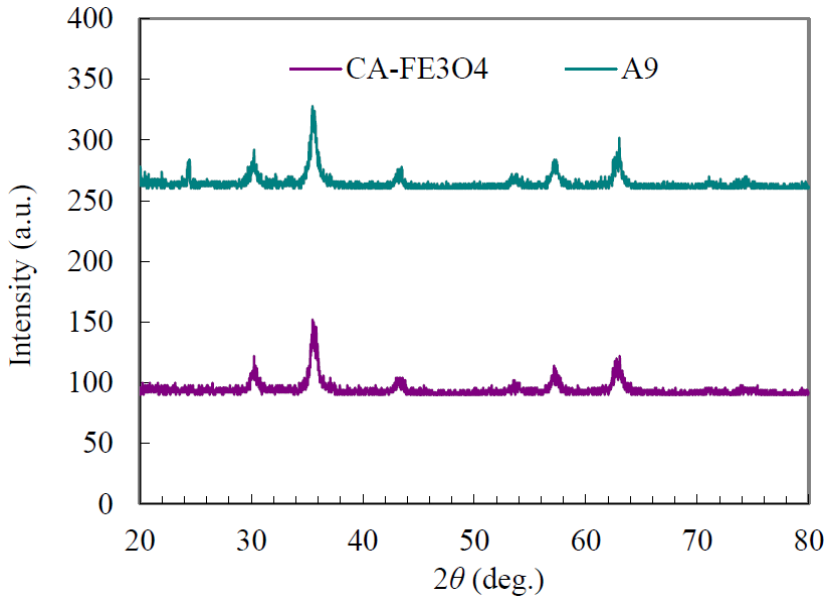

Figure 9. XRD patterns of the A9 sample (the DC coated Fe_3O_4 MNPs) and the CA coated Fe_3O_4 MNPs.

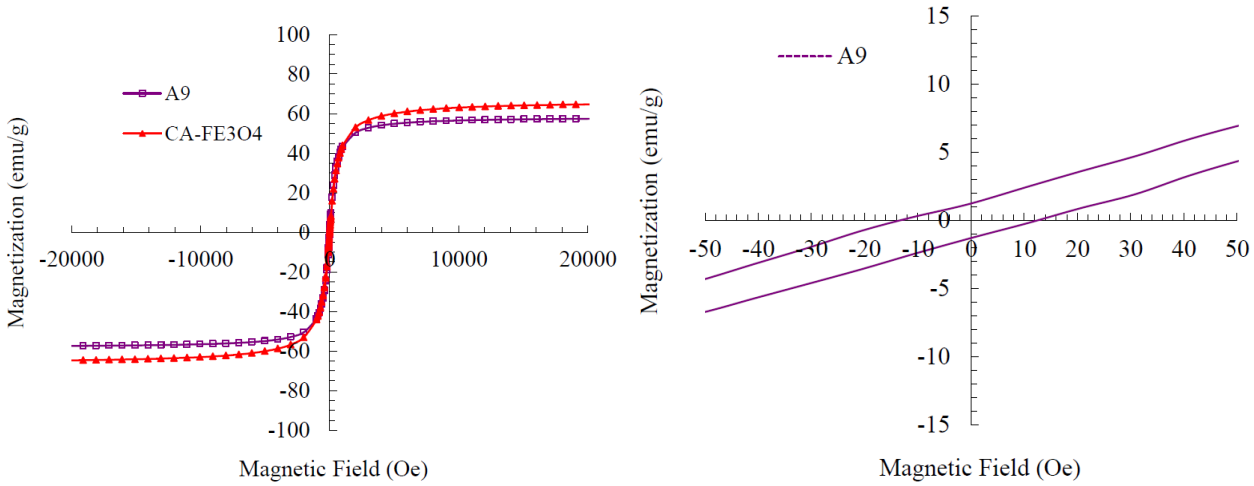

Figure 10. Magnetization curves (a) of the DC coated Fe_3O_4 MNPs as the A9 sample and the CA coated Fe_3O_4 MNPs. The coercivity (Hc) and remanent magnetization (Mr) of A9 (b).

3.3. Heating effect of the DC coated Fe_3O_4 FFs

FF can be used for the magnetic inductive heating treatment of tumor, and one of the crucial

factors is that the temperature used for cancer therapy should reach 44~47 ℃. In this section, the A9 samples with different concentrations were prepared. Super-high frequency inductive heating equipment (power-rise highfrequency machine Co. Ltd., Taiwan) with whole power output of 7 kW was used in this heating treatment of FFs [17]. The frequency applied in the present work was 45 kHz. The digital thermometer with a resolution of 0.01 ℃ was used for temperature measurement. The volume of FF was 2 ml, and temperature probe was placed in the center and middle (height as the place of 1 ml) of the volumetric cylinder. For the comparisons with the previous study in [17], it is noted that the heating effects due to the FF concentration and the magnetic field intensity were shown and discussed, respectively.

Firstly, the heating effect due to the influence of the FF concentration was investigated. From Figure 11, we could see that the temperature of DC coated FFs (the A9 sample) with different concentrations of 2 mg/ml and 50 mg/ml in an alternating electrical current of 210 A (AC field amplitude in the 0.087 kA/m or 0.11 mT), rose sharply in 10 s. The temperature of 2 mg/ml sample rose to 52.71 ℃ from 33.30 ℃ in 5 s (the temperature increase was 19.41 ℃ and the rise rate of temperature was 5.14 ℃/s by the approximation of six-order polynomial curve), while the temperature of 50 mg/ml sample rose to 53.42 ℃ from 33.15 ℃ in 5 s (the temperature increase was 20.27 ℃ and the rise rate of temperature was 5.22 ℃/s by the approximation of six-order polynomial curve). In addition, for the CA coated FF with a concentration of 50 mg/ml in an alternating electrical current of 210 A, the temperature rose to 58.41 ℃ from 33.86 ℃ in 5 s, The temperature increase was 24.55 ℃, which was higher than that of the DC coated FF with a concentration of 50 mg/ml, as shown in Figure 11.

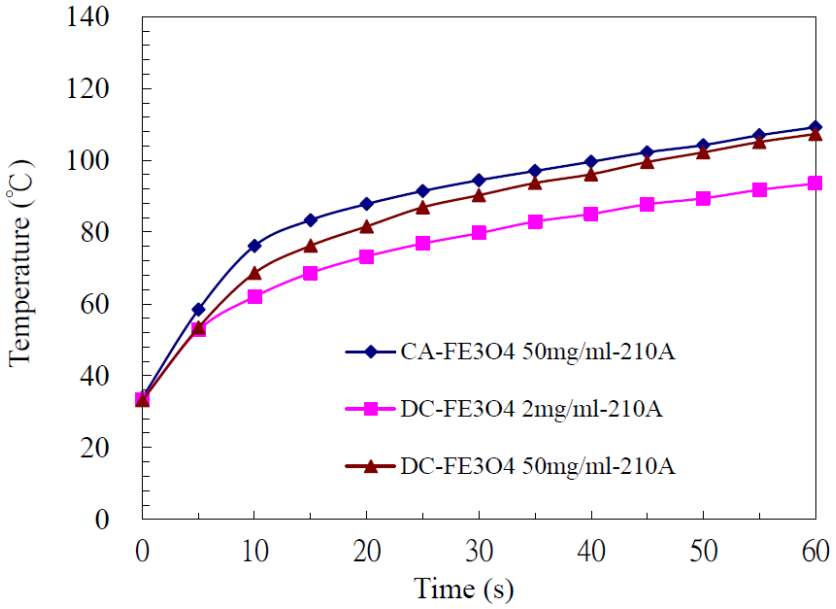

Figure 11. Temperature rise of FFs under AC magnetic field, the CA coated FF and the DC coated FFs with different concentrations in an alternating electrical current of 210 A.

In FFs (magnetic fluids), heating effects can be achieved in AC magnetic fields due to Néel-type relaxation loss or energy dissipation during particle rotation in liquid (Brown loss) [16]. With the Brownian mechanism of relaxation the magnetic moment is locked to the crystal axis and when the

magnetic moment aligns with the field, the particle rotates as well. A second mechanism exists (Néel relaxation) in which the magnetic moment rotates within the crystal [32]. This type of mechanism (relaxation) is dominant in magnetic fluids with single-domain magnetite particles that do not exceed a diameter of 46 nm [16,33]. For larger magnetic particles the role of the hysteresis loss mechanism increases [33] due to the strongly size-dependent coercivity H_C.

Further, the coercivity is dependent on the particle size, which was emphasized [34]. There is a critical size below which it costs more energy to create a domain wall than to support the external magnetostatic energy of the single-domain state. Above the critical size, multi-domain magnetism begins in which a smaller reversal magnetic field is required to make the net magnetization zero. Generally, at the size smaller than 20 nm for spherical NPs, a ferromagnetic NP often contains a single domain. As the size of these single-domain particles decreases, the coercivity decreases. When ferromagnetic NP size is continually decreased to a level where the magnetic anisotropy energy (KV, K is bulk magneto crystalline anisotropy, V is NP volume) is smaller than the thermal energy (k_BT, k_B is the Boltzmann constant, T is temperature), the MNP is said to be superparamagnetic. At superparamagnetic state, MNP shows no Hc or Mr; thus, the magnetic dipole-dipole interaction is minimized [34].

Additionally, the basic concepts of magnetism and the physics of the hyperthermia process were reviewed in details [35]. Rosensweig studied the mechanism of heat generation in a magnetic fluid due to a variable magnetic field and developed dissipation relationships based on the rotational relaxation of single-domain MNP dispersed in a liquid matrix [32]. These particles are assumed to be less than 20 nm in diameter, so eddy current heating can be neglected [32,35]. Rosensweig found that there is strong size dependence in the heating rate [32]. The size of the particle affects the time constant of each relaxation mechanism: the larger the particles are, the larger the Brownian and Néel relaxation time constant will be. The dominating contribution will be by the faster relaxation time [35].

Moreover, a comparative study was proposed for the specific loss power (SLP) generated by an external magnetic field in superparamagnetic as well as ferromagnetic magnetite particles suspended in molten and solidified gel [36]. For superparamagnetic fluids, a "H^2 law" was observed for the specific absorption rate (SAR = (C/m)·($\Delta T/\Delta t$), where C is the sample specific heat capacity, m is the sample mass) dependence on the amplitude of the magnetic field [16,36]. SAR (also known as SLP) is quite often used in the literature to characterize the heating ability of MNPs; it has a significant limitation in that it is an extrinsic (equipment-specific) parameter. The SAR parameter for the same magnetic fluid will change when measured in AC magnetic field systems with different frequencies and strengths, Therefore the "intrinsic loss power, ILP" as a new design rule parameter is introduced [37] and is defined as SAR/H^2f.

In our previous study, heating effect of the FF without coating (agglomerations) was caused by magnetic hysteresis loss (induced by the size-dependent covercivity) and temperature rise was slow than that in the CA coated FF [4]. Stability and relaxation mechanisms of CA coated magnetite NPs for magnetic hyperthermia were discussed [38]. From the outlined stabilization ways emerges the possibility of either using MNPs with large hydrodynamic sizes (polymeric like coating, steric stabilization) possibly resulting in a Néel driven process or using MNPs covered with small organic molecules as CA (combined electrostatic and steric stabilization), which may dissipate through a Brown type process [38]. Accordingly, the question of which of these mechanisms optimizes the heating process is still an open question, whose answer requires more experimental research [38]. It

was indicated that dipolar interactions between the NPs play a key role in the Néel relaxation mechanism and dissipation efficiency. Magnetic relaxation becomes slower for interacting colloids, and heating efficiency increases. The largest SAR values arise from the more interacting NPs, a case where Néel relaxation times become larger than Brown relaxation times, leading the Brown dissipation mechanism to prevail [38].

In this study, the superparamagnetic CA coated and DC coated MNPs were obtained of high saturation magnetization with low coercivity. For these MNPs, heat generated by the hysteresis loss was very small because of their superparamagnetic properties. Hence heating effect of the CA coated FFs and the DC coated FFs could be achieved in AC magnetic field due to Néel-type relaxation loss and/or energy dissipation during particle rotation in viscous liquid (Brown loss) [16]. On the same condition of 50 mg/ml and under 210 A, the temperature rise for the CA coated FF was higher than that of the DC coated FF, as shown in Figure 11, which was highly connected with the excellent dispersion and higher saturation magnetization in the CA coated FF. In the physical mechanism, Brown loss might dominate the power dissipation in the CA coated FF.

Generally speaking, heating effect of materials was influenced by many factors, such as size, structure, morphologies, etc. The heat generated by FFs was equal to the amount of heat emitted to the environment, so the temperature would not rise with the increasing time [17]. Compared to the results in [17], the time for temperature of the DC coated FF (the A9 sample with 2 mg/ml in 210 A) increased up to 47 ℃ was much shorter than that of 200 s, which was found for the sodium oleate coated Fe_3O_4 FF, in the case of the same concentration of 2 mg/ml and applied current of 210 A [17], and was shorter than that of 76 s, which was found for the CA coated Fe_3O_4 FF, in the case of the same concentration of 2 mg/ml and applied current of 300 A [4].

Subsequently, heating effect due to the influence of the magnetic field intensity was investigated. Heating tests of the A9 sample (the DC coated FF with 2 mg/ml) were carried out in different currents from 120 A to 210 A. As shown in Figure 12, with the increase in electrical current, the temperature of the FF increased rapidly. When the electrical current was 120 A, the final temperature could be as high as 77.14 ℃ in 60 s. However, when the electrical current was increased to 150 A, the temperature rose to 84.05 ℃ in 60 s, whereas the final temperature was 93.52 ℃ in 60 s when the electrical current was 210 A. The results indicated that magnetic field intensity had great influence on the final temperature and the rise rate of temperature increased with the increasing magnetic field intensity. The stronger the intensity of the magnetic field, the higher the temperature of the FF [39]. It was noted that the initial temperature was set as room temperature around 33 ℃, and the temperature rose over 47 ℃ in 5 s for these applied electrical currents, respectively.

In the recent researches of magnetic fluid hyperthermia (MFH), it is noted that the frequency range is usually 10~200 kHz, the magnetic field range is 0~15 kA/m, and the temperature rise is required to increase quickly within 5~15 min [40]. Further, the value obtained by the multiplication of frequency and magnetic field intensity is not more than 4.85×10^8 $Am^{-1}s^{-1}$ for the human safety [41]. In our study, the *Hf* was 3.92×10^6 $Am^{-1}s^{-1}$ (45 kHz × 0.087 kA/m, under 210 A) and below 4.85×10^8 $Am^{-1}s^{-1}$. When the electrical current was 210 A , the temperature rise was 19.41 ℃ for the DC coated FF (A9) with 2 mg/ml and was higher than that of 16.62 ℃ for the dextran stabilized FF with unknown concentration [16].

In future work, we will focus on the stability (pH-dependent Zeta potential) in single/double-layer coated MNPs with different sizes, and aim to find the optimum size with a high heating efficiency in applied magnetic field [42]. Further, the double-layer coated CA and PEG FFs for

biomedical applications was considered. Especially, the corresponding SAR value is to be calculated (weight of the magnetic phase of the NPs per cc of the sample is needed to be measured before the calculation) and to make comparisons with other published high SAR values [43].

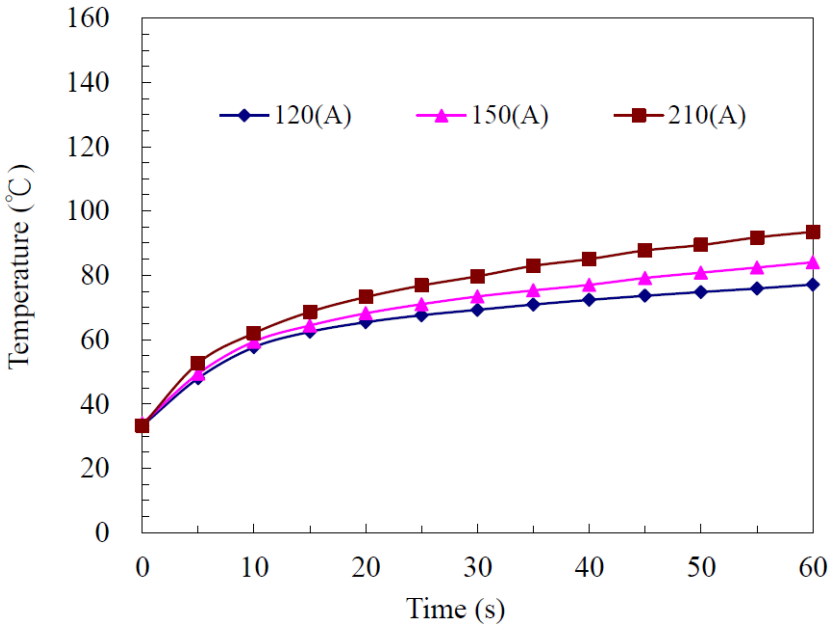

Figure 12. Temperature rise of FFs under AC magnetic field, the heating tests of 2 mg/ml DC coated FF in different electrical currents from 120 A to 210 A.

4. Conclusions

The Fe_3O_4 MNPs coated by citric acid and dextran were prepared by the co-precipitation method. Via the tests of DLS and SQUID, the dextran-citrate coated Fe_3O_4 FF with 0.6 g dextran was characterized with low PDI as 0.153 and with high saturation magnetization of 60.07 emu/g. The optimized DC coated FF as the A9 sample obtained by uniform design method, its retardance was measured as high as 56.7898° (dichroism was 0.3716) under 64.5 mT. Further, heating effect for A9 with different concentrations was investigated. When the concentrations were of 2 mg/ml and 50 mg/ml, under the external alternating magnetic field with applied apparent current of 210 A, after only 5 s, the temperature of FFs was greater than 47 ℃, respectively, reached the requirements for the heating treatment of medicinal cancer tumor. Therefore, the potential in hyperthermia for DC coated FFs was highly evaluated in this study.

Acknowledgements

The financial support provided to this study by the Ministry of Science and Technology in Taiwan under Grant MOST 104-2221-E-269-006 is gratefully acknowledged.

Conflict of Interest

There is no conflict of interest in publishing the research findings and in publishing the results.

References

1. Mehta RV, Desai R, Bhatt P, et al. (2006) Synthesis and characterization of certain nonmagnetic particles coated with citrate and dextran molecules. *Indian J Pure Appl Phys* 44: 537–542.
2. Hong RY, Feng B, Chen LL, et al. (2008) Synthesis, characterization and MRI application of dextran-coated Fe_3O_4 magnetic nanoparticles. *Biochem Eng J* 42: 290–300.
3. Cheraghipour E, Javadpour S, Mehdizadeh AR (2012) Citrate capped superparamagnetic iron oxide nanoparticles used for hyperthermia therapy. *J Biomed Sci Eng* 5: 715–719.
4. Lin JF, Tsai CC (2016) Synthesis of citrate coated ferrofluids with high magnetic heating. Proceedings of the 2015 International Conference on Mechanics and Mechatronics, 95–103.
5. Srivastava S, Awasthi R, Gajbhiye NS, et al. (2011) Innovative synthesis of citrate-coated superparamagnetic Fe_3O_4 nanoparticles and its preliminary applications. *J Colloid Interf Sci* 359: 104–111.
6. Saraswathy A, Nazeer SS, Jeevan M, et al. (2014) Citrate coated iron oxide nanoparticles with enhanced relaxivity for in vivo magnetic resonance imaging of liver fibrosis. *Colloid Surface B* 117: 216–224.
7. Li L, Mak KY, Leung CW, et al. (2013) Effect of synthesis conditions on the properties of citric-acid coated iron oxide nanoparticles. *Microelectron Eng* 110: 329–334.
8. Lin JF, Tsai CC, Lee MZ (2014) Linear birefringence and dichroism in citric acid coated Fe_3O_4 magnetic nanoparticles. *J Magn Magn Mater* 372: 147–158.
9. Gravinaa PP, Santos JS, Figueiredo LC, et al. (2002) Biocompatible magnetic fluids: A comparative birefringence investigation. *J Magn Magn Mater* 252: 393–395.
10. Lattuada M, Hatton T (2007) Preparation and controlled self-assembly of janus magnetic nanoparticles. *J Am Chem Soc* 129: 12878–12889.
11. Mornet S, Portier J, Duguet E (2005) A method for synthesis and functionalization of ultrasmall superparamagnetic covalent carriers based on maghemite and dextran. *J Magn Magn Mater* 293: 127–134.
12. Cheraghipour E, Tamaddon AM, Javadpour S, et al. (2013) PEG conjugated citrate-capped magnetite nanoparticles for biomedical applications. *J Magn Magn Mater* 328: 91–95.
13. Hong RY, Li JH, Qu JM, et al. (2009) Preparation and characterization of magnetite/dextran nanocomposite used as a precursor of magnetic fluid. *Chem Eng J* 150: 572–580.
14. Hauser AK, Mathias R, Anderson KW, et al. (2015) The effects of synthesis method on the physical and chemical properties of dextran coated iron oxide nanoparticles. *Mater Chem Phys* 160: 177–186.
15. Xu XQ, Shen H, Xu JR, et al. (2005) Core-shell structure and magnetic properties of magnetite magnetic fluids stabilized with dextran. *Appl Surf Sci* 252: 494–500.
16. Józefczak A, Skumiel A (2007) Study of heating effect and acoustic properties of dextran stabilized magnetic fluid. *J Magn Magn Mater* 311: 193–196.
17. Lin JF, Tsai CC, Huang CH, et al. (2015) Magneto-optical properties and magnetic inductive heating of sodium oleate coated Fe_3O_4 magnetic fluid. *Optik* 126: 907–911.
18. Lin JF, Lee MZ (2012) Concurrent measurement of linear birefringence and dichroism in ferrofluids using rotating-wave-plate Stokes polarimeter. *Opt Commun* 285: 1669–1674.
19. Lin JF, Sheu JJ, Lee MZ, et al. (2014) Linear birefringence and dichroism measurements for silica coated iron oxide ferrofluids. *IEEE T Magn* 50: 4001904.

20. Swierczewska M, Han HS, Kim K, et al. (2016) Polysaccharide-based nanoparticles for theranostic nanomedicine. *Adv Drug Deliver Rev* 99: 70–84.
21. Barrow M, Taylor A, Murray P, et al. (2015) Design considerations for the synthesis of polymer coated iron oxide nanoparticles for stem cell labelling and tracking using MRI. *Chem Soc Rev* 44: 6733–6748.
22. Lima-Tenório MK, Gómez Pineda EA, Ahmad NM, et al. (2015) Magnetic nanoparticles: In vivo cancer diagnosis and therapy. *Int J Pharmaceut* 493: 313–327.
23. Herrera A, Rodríguez H, Torres-Lugo M, et al. (2006) Functionalization of Magnetite (Fe_3O_4) Nanoparticles for Cancer Treatment. *NSTI-Nanotech* 2: 75–78.
24. Song J, Song Z, Sun R (2012) Study of uniform experiment design method applying to civil engineering. *Procedia Eng* 31: 739–745.
25. Fang KT (1994) *Uniform Design and Uniform Design Tables*, Beijing: Science Press.
26. Liang YZ, Fang KT, Xu QS (2001) Uniform design and its applications in chemistry and chemical engineering. *Chemometr Intell Lab* 58: 43–57.
27. Yang XQ (2006) Study on the liver targeted pro-drug of magnetic dextran-mitomycin nanoparticles [PhD Dissertation]. The First Military Medical University.
28. Rong Z, Enjuan Z (1999) Uniform design and its application in pharmaceutics: A review. *Acta Academic Medicnae Militaris Tertiae* 21: 1–5.
29. Hong RY, Pan TT, Han YP, et al. (2007) Magnetic field synthesis of Fe_3O_4 nanoparticles used as a precursor of ferrofluids. *J Magn Magn Mater* 310: 37–47.
30. Easo SL, Mohanan PV (2013) Dextran stabilized iron oxide nanoparticles: Synthesis, characterization and *in vitro* studies. *Carbohyd Polym* 92: 726–732.
31. Lin JF, Wang CH, Lee MZ, et al. (2013) Linear birefringence and dichroism measurement in oil-based Fe_3O_4 magnetic nanoparticles. *J Magn Magn Mater* 332: 192–198.
32. Rosensweig RE (2002) Heating magnetic fluid with alternating magnetic field. *J Magn Magn Mater* 252: 370–374.
33. Ma M, Wu Y, Zhou J, et al. (2004) Study of heating effect and acoustic properties of dextran stabilized magnetic fluid. *J Magn Magn Mater* 268: 33–39.
34. Liu XL, Fan HM (2014) Innovative magnetic nanoparticle platform for magnetic resonance imaging and magnetic fluid hyperthermia applications. *Curr Opin Chem Eng* 4: 38–46.
35. Laurent S, Dutz S, Häfeli UO, et al. (2011) Magnetic fluid hyperthermia: Focus on superparamagnetic iron oxide nanoparticles. *Adv Colloid Interf Sci* 166: 8–23.
36. Hiergeist R, Andrä W, Buske N, et al. (1999) Application of magnetite ferrofluids for hyperthermia. *J Magn Magn Mater* 201: 420–422.
37. Kallumadil M, Tada M, Nakagawa T, et al. (2009) Suitability of commercial colloids for magnetic hyperthermia. *J Magn Magn Mater* 321: 1509–1513.
38. Sousa M, Raap M, Rivas PC, et al. (2013) Stability and relaxation mechanisms of citric acid coated magnetite nanoparticles for magnetic hyperthermia. *J Phys Chem C* 117: 5436–5445.
39. Wang YM, Cao X, Liu GH, et al. (2011) Synthesis of Fe_3O_4 magnetic fluid used for magnetic resonance imaging and hyperthermia. *J Magn Magn Mater* 323: 2953–2959.
40. Moroz P, Jones SK, Gray BN, et al. (2002) Magnetic medical hyperthermia: current status and future direction. *Int J Hyperther* 18: 267–284.
41. Atkinson WJ, Brezovich IA, Chakraboty DP (1984) Usable frequencies in hyperthermia with thermal seeds. *IEEE T Biomed Eng* 31: 70–75.

42. Li Z, Kawashita M, Araki N, et al. (2010) Magnetite nanoparticles with high heating efficiencies for application in the hyperthermia of cancer. *Mater Sci Eng C* 30: 990–996.
43. Lahiri BB, Muthukumaran T, Philip J (2016) Magnetic hyperthermia in phosphate coated iron oxide nanofluids. *J Magn Magn Mater* 407: 101–113.

AIMS Press